Non-blocking four-port optical router based on thermo-optic silicon microrings*

DANG Pei-pei (党佩佩), **LI Cui-ting** (李翠婷), **ZHENG Wen-xue** (郑文雪), **ZHENG Chuan-tao** (郑传涛)**, **and WANG Yi-ding** (王一丁)

State Key Laboratory on Integrated Optoelectronics, College of Electronic Science and Engineering, Jilin University, Changchun 130012, China

(Received 27 April 2016)

By using silicon-on-insulator (SOI) platform, 12 channel waveguides, and four parallel-coupling one-microring resonator routing elements, a non-blocking four-port optical router is proposed. Structure design and optimization are performed on the routing elements at 1 550 nm. At drop state with a power consumption of 0 mW, the insertion loss of the drop port is less than 1.12 dB, and the crosstalk between the two output ports is less than −28 dB; at through state with a power consumption of 22 mW, the insertion loss of the through port is less than 0.45 dB, and the crosstalk between the two output ports is below −21 dB. Routing topology and function are demonstrated for the four-port optical router. The router can work at nine non-blocking routing states using the thermo-optic (TO) effect of silicon for tuning the resonance of each switching element. Detailed characterizations are presented, including output spectrum, insertion loss, and crosstalk. According to the analysis on all the data links of the router, the insertion loss is within the range of 0.13—3.36 dB, and the crosstalk is less than −19.46 dB. The router can meet the need of large-scale optical network-on-chip (ONoC).

Document code: A **Article ID:** 1673-1905(2016)04-0268-5

DOI 10.1007/s11801-016-6105-3

As the continuous development of semiconductor technologies, both on-chip communication capacity and speed increase. To meet the pressing demand for extremely high bandwidth, low power consumption, excellent performance, and good scalability, optical network-on-chip (ONoC) is emerging as a new paradigm to interconnect a great number of processing cores at chip level. Many ONoCs with different architectures have been proposed, such as the photonic NoC with hybrid architecture[1], 3D optical NoC[2], torus-based hierarchical hybrid optical-electronic NoC[3], diagonal mesh NoC[4], etc. As the most important element in photonic NoC, optical router, which generally comprises optical switches and waveguides, has received more and more attention. According to topological structure, it can be divided into single-stage and multi-stage structures[5-7]; according to port number, it can be divided into four-, five-, eight-, and *N*-port optical routers[8-11]; according to basic routing element, it can be divided into micro-ring resonators (MRRs), Mach-Zehnder interferometer (MZI) based routers[12,13]; according to being controlled or not, it can be divided into active and passive optical routers[14,15]. Within the available structures, MRRs are typically preferred due to their ultra-compact size, simple-mode resonances, and ease of phase-matching between an MRR and its coupling waveguides. Besides, the MRR structure is more convenient for building large switching arrays by cascading fundamental elements. Therefore, a non-blocking four-port optical router is proposed in this paper, by using only four parallel-coupling one-microring resonator routing elements.

The topology of the router is shown in Fig.1(a), which consists of 12 channel waveguides and four groups of parallel-coupling one-microring crossing resonators (PCO-MRRs). The basic routing elements are numbered from S_1 to S_4. The router is designed to be operated at the wavelength of 1 550 nm. All the rings are with the same radius, and without heating, the ring resonates at 1 550 nm, and all the four elements have the same length and width. Except for the waveguide crossing for making I_i and O_i (i=1—4) have the same physical address and the waveguide crossing of the basic routing elements, there is no waveguide crossing for cascading the elements. The structure of the basic routing switch element is shown in Fig.1(b). It has the function of routing a signal from input port to two different output ports via controlling the cou-

* This work has been supported by the National Natural Science Foundation of China (Nos. 61107021 and 61177027), the Ministry of Education of China (Nos.20110061120052 and 20120061130008), the China Postdoctoral Science Foundation (Nos.20110491299 and 2012T50297), the Science and Technology Department of Jilin Province of China (No.20130522161JH), and the Special Funds of Basic Science and Technology of Jilin University (No.201103076).

** E-mail: zhengchuantao@jlu.edu.cn

pling between channel waveguide and MRR waveguide. The basic routing element has one waveguide crossing, its two input ports I_1 and I_2 are located at one side, and its two output ports O_1 and O_2 are located at the other side. The cross section between MRR waveguide and channel waveguide is shown in Fig.1(c). The core material of the rectangle waveguide is silicon, and the cladding material is silica. The electrode heater TiN with a width of W is only deposited upon the MRR waveguide, and the channel waveguide is passive without electrode. The thicknesses of the two waveguides are both t_1, and the two waveguide core widths (w_c for channel and w_r for MRR) are slightly different to make the propagation constants identical under the case of without heating on electrode. For decreasing the waveguide crossing loss, the crossing point of the two waveguides is intensively designed, as shown in the inset of Fig.1(b). Two wide waveguides cross together, and the narrow and wide waveguides connect with each other through a short transitive region.

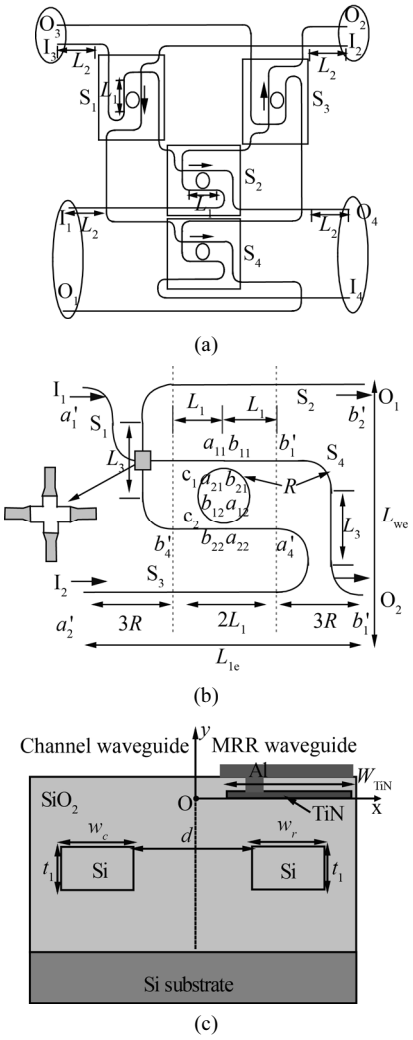

Fig.1 (a) Optical interconnection network of the four-port optical router; (b) Structure of the parallel-coupling one-microring crossing resonator; (c) Cross section between MRR waveguide and channel waveguide

The under silica cladding layer thickness is 2 μm, and the thickness of the upper silica cladding layer that can be deposited on the silicon core layer by plasma enhanced chemical vapor deposition (PECVD) is 1.5 μm. The heater is TiN that can be sputtered on the upper silica layer, its thickness is h_{TiN}=200 nm, and its width is W_{TiN}=0.4 μm. The heating voltage is realized by directly imposing a voltage on the Ω-shape aluminum electrode deposited on top of the device. Without considering the influence of bending on mode constants, Fig.2(a) shows the relations between effective refractive indices of E_{00}^y, E_{01}^y and E_{10}^y modes versus MRR waveguide core width w_r, where the core thickness and width are equal, that is, w_r=t_1. It can be found that the single mode condition is 0.3 μm<w_r=t_1<0.4 μm, and we select w_r=t_1=0.35 μm. The influence of bending on E_{00}^y mode refractive index is further considered, as shown in Fig.2(a). It can be shown that the difference between the two cases of considering and without considering bending effect is not obvious. When $w_r \leq 0.7$ μm, the two curves are almost overlapped with each other; whereas only when w_r gets large enough, they appear to be slightly different. Considering bending effect, the mode effective index is n_r=2.387 5 with w_r=0.35 μm. For the channel waveguide, the core thickness is equal to that of the MRR waveguide, which is 0.35 μm. Without heating on the electrode, the mode effective indices of the two waveguides should be identical for phase matching. Fig.2(a) also presents the curve of effective index of E_{00}^y mode versus the channel waveguide core width w_c. For enabling the two effective indices to be identical, we also choose w_c=0.35 μm.

The bending radius R should satisfy the resonance equation $2\pi R n_r = m\lambda$, where m is resonance order. Fig.2(b) shows the curves of fundamental mode effective index n_r and bending radius R versus resonance order m, where w_r=t_1=0.35 μm, and the upper/under confined layers are assumed to be half-infinite. As m increases, n_r decreases, and R increases. Properly, we select m=120, and the bending radius is determined to be R=12.4 μm. On the other hand, the bending will cause extra bending loss. When R=12.4 μm, the bending loss coefficient is far below 10^{-4} dB/cm, which can be neglected in calculation.

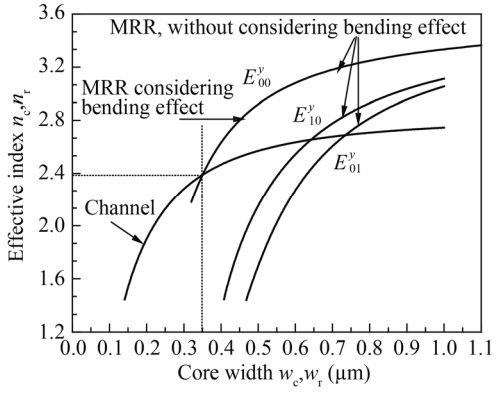

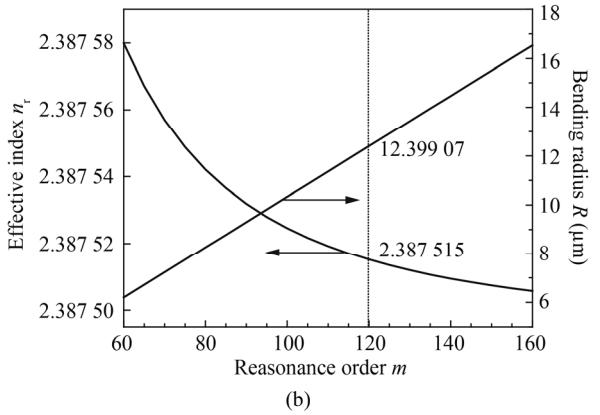

Fig.2 (a) At 1 550 nm wavelength, curves of mode effective indices of MRR waveguide and channel waveguide versus waveguide core width; (b) At 1 550 nm wavelength, curves of fundamental mode effective index n_r and bending radius R versus resonance order m

Take L_1=30 μm, L_2=100 μm, L_3=2d+2R+w_c+w_r ≈ 27 μm. Through optimization, the footprint size of the element is (2L_1+6R)(i.e., L_{le})×(2L_3+2R)(i.e., L_{we})=114 μm×77 μm. Then we can estimate the footprint size of the router as (L_{le}+2L_{we}+4R+2L_2)×(L_{le} +2L_{we}+7R) =377.3 μm×354.5 μm.

Under the resonance wavelength of 1 550 nm, for the basic routing element, Fig.3 shows the curves of output power P_{o1} and P_{o2} versus temperature increase of the heater ΔT under two input cases. It can be found that when ΔT=0 K, under two different conditions, the resonators are all operated at drop state, the insertion losses are 1.12 dB and 0.72 dB, and the crosstalks between the two ports are −28.76 dB and −28.78 dB, respectively. As the increase of temperature, the mode mismatch between the channel waveguide and MRR waveguide is enhanced, the output power from the resonance port drops, and the output power from the through port (non-resonant port) increases. When ΔT=40 K, the crosstalks between the two ports are below −21.39 dB and −21.38 dB, and the insertion losses of the through port are about 0.45 dB and 0.07 dB, respectively. When ΔT=40 K, the power consumption is about 22 mW.

In two kinds of working conditions, since the basic routing element shows the same routing function, we only analyze the spectrum under the condition of a_{22}=0. Within the temperature increase from 0 K to 40 K, curves of output power from the on port and off port versus input light wavelength are presented in Fig.4. Under the operation wavelength of 1 550 nm, when the applied power is 0 mW (0 K), the input power into the port I_1 will fully output from the drop port (O_1) through the coupling with microrings, the device reveals resonate-state, and the crosstalk is less than −28.76 dB. When the applied power is 22 mW (40 K), the output power from the drop port drops from point c to d, and that of the through port increases from point b to a. This state is named through-state, and the crosstalk is less than −21.39 dB.

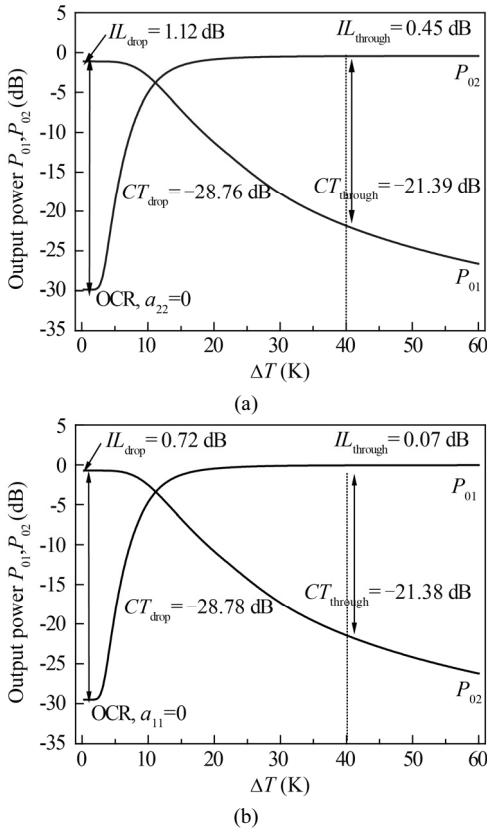

Fig.3 Curves of output power versus the temperature increase of the waveguide for the basic routing element working under (a) the light input into port I_1, and (b) the light input into port I_2, where the operation wavelength is taken as 1 550 nm

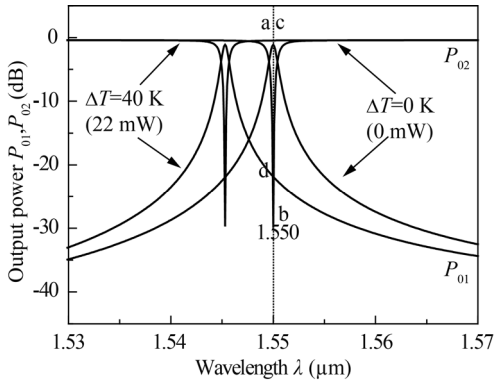

Fig.4 Curves of output power from ports O_1 and O_2 versus light wavelength within the range of 1.53—1.57 μm for the basic routing element, with the light input into port I_1

To demonstrate the non-blocking routing operation of the four-port optical router, all of the possible data links are analyzed here. Let four light wave beams with 1 550 nm wavelength input into the four ports simultaneously, which can output from different ports. Excluding the U-turn operation, there are nine routing states in total. Tab.1 shows all the routing paths, which can be selected by making the four microrings at through state

(T) or drop state (D). So, once the router is used in an ONoC, it can be set to be the required operation state through control electronics. For example, when the four-port optical router works at the first routing state in Tab.1, the optical links from input port to output port are $I_1 \rightarrow O_2$, $I_2 \rightarrow O_1$, $I_3 \rightarrow O_4$, and $I_4 \rightarrow O_3$, and S_1—S_4 should work at through state.

Typically, along the 36 paths of the four-port optical router under the nine routing states, the output spectra of all output ports relative to corresponding input ports are calculated and shown in Fig.5. Under definite operation states, the 1 550 nm wavelength can output from the desired port.

Based on the calculation results in Fig.5, the insertion losses of all data-links are determined and shown in Tab.2. The insertion losses of all data links are determined to be within the range of 0.13—3.36 dB. We also calculate the crosstalks of the 36 data-links under the nine routing states, which are also depicted in Tab.1. The crosstalk is found to be less than −19.46 dB.

Tab.1 Routing paths and operation states of the four switch elements

Routing states	Input ports				Operation states of switch elements			
	I_1	I_2	I_3	I_4	S_1	S_2	S_3	S_4
1	O_2	O_1	O_4	O_3	T	T	T	T
2	O_2	O_3	O_4	O_1	T	T	T	D
3	O_2	O_4	O_1	O_3	D	T	T	T
4	O_3	O_1	O_4	O_2	T	T	D	T
5	O_3	O_4	O_1	O_2	D	T	D	T
6	O_3	O_4	O_2	O_1	D	T	D	D
7	O_4	O_1	O_2	O_3	T	D	T	T
8	O_4	O_3	O_1	O_2	D	D	D	T
9	O_4	O_3	O_2	O_1	D	D	D	D

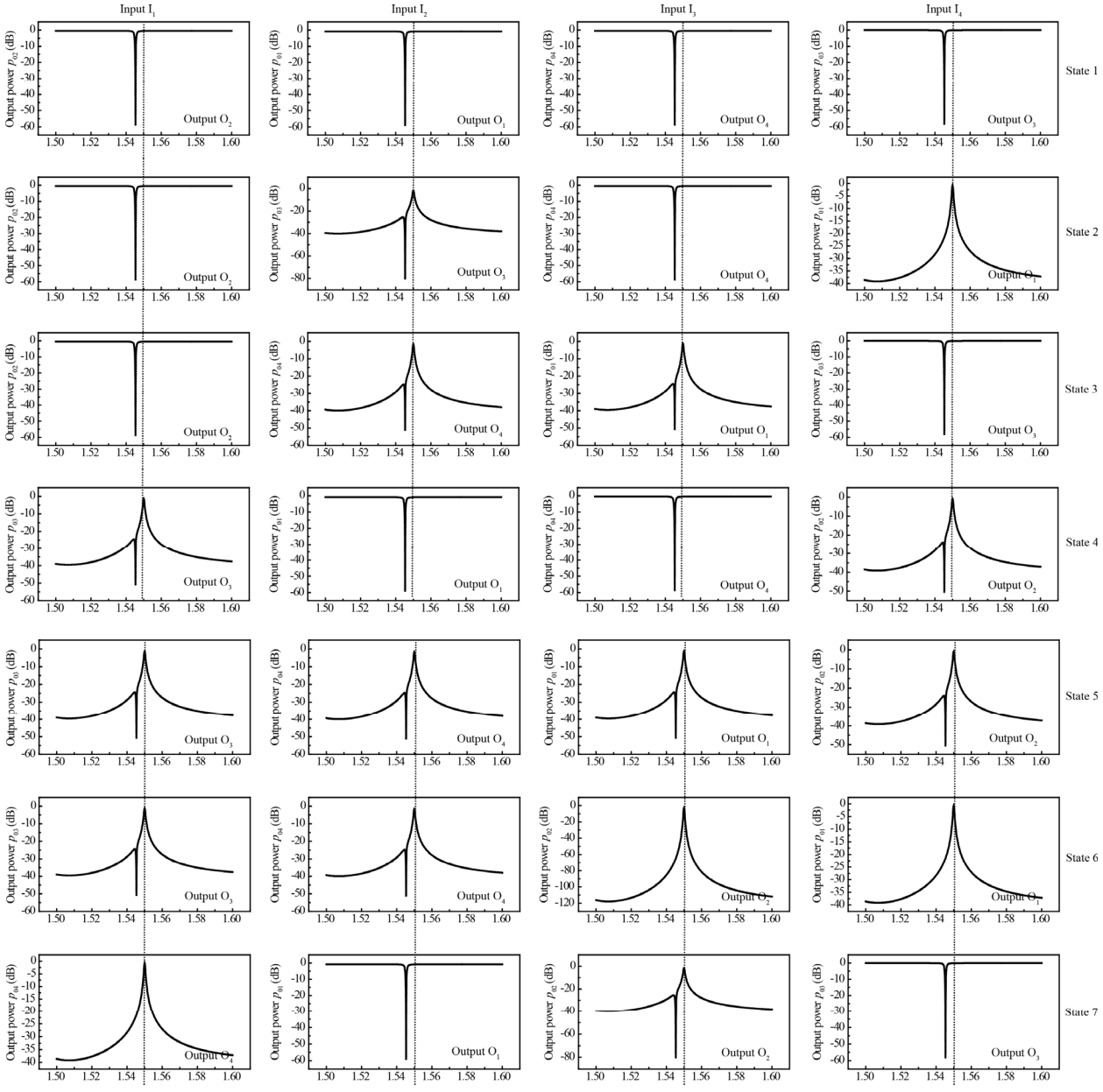

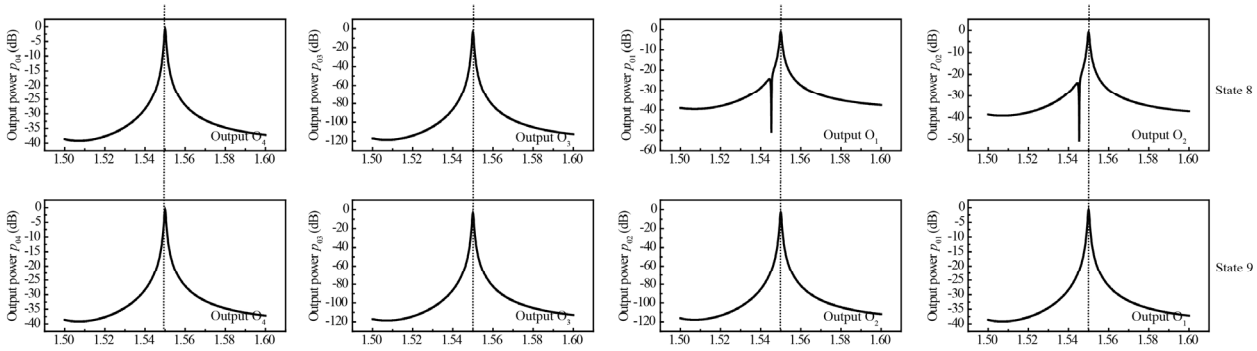

Fig.5 Optical spectra of 36 routing paths of the four-port optical router under 9 routing states

Tab.2 The crosstalk and insertion loss results of 36 data-links under the 9 routing states of the four-port optical router (CT: crosstalk, IL: insertion loss; Unit: dB)

State 1	Data link	$I_1 \rightarrow O_2$	$I_2 \rightarrow O_1$	$I_3 \rightarrow O_4$	$I_4 \rightarrow O_3$
	CT, IL	−20.13, 0.52	−21.39, 0.91	−20.58, 0.52	−20.11, 0.13
State 2	Data link	$I_1 \rightarrow O_2$	$I_2 \rightarrow O_3$	$I_3 \rightarrow O_4$	$I_4 \rightarrow O_1$
	CT, IL	−20.13, 0.52	−20.26, 1.64	−21.71, 0.52	−30.04, 0.72
State 3	Data link	$I_1 \rightarrow O_2$	$I_2 \rightarrow O_4$	$I_3 \rightarrow O_1$	$I_4 \rightarrow O_3$
	CT, IL	−20.13, 0.52	−21.85, 1.57	−21.86, 1.17	−20.11, 0.13
State 4	Data link	$I_1 \rightarrow O_3$	$I_2 \rightarrow O_1$	$I_3 \rightarrow O_4$	$I_4 \rightarrow O_2$
	CT, IL	−19.46, 1.19	−21.39, 0.91	−20.58, 0.52	−20.26, 0.79
State 5	Data link	$I_1 \rightarrow O_3$	$I_2 \rightarrow O_4$	$I_3 \rightarrow O_1$	$I_4 \rightarrow O_2$
	CT, IL	−19.46, 1.19	−22.51, 1.57	−21.71, 1.17	−20.26, 0.79
State 6	Data link	$I_1 \rightarrow O_3$	$I_2 \rightarrow O_4$	$I_3 \rightarrow O_2$	$I_4 \rightarrow O_1$
	CT, IL	−19.46, 1.19	−22.51, 1.57	−28.44, 2.56	−29.90, 0.72
State 7	Data link	$I_1 \rightarrow O_4$	$I_2 \rightarrow O_1$	$I_3 \rightarrow O_2$	$I_4 \rightarrow O_3$
	CT, IL	−30.03, 0.72	−21.86, 0.91	−19.46, 1.64	−20.11, 0.13
State 8	Data link	$I_1 \rightarrow O_4$	$I_2 \rightarrow O_3$	$I_3 \rightarrow O_1$	$I_4 \rightarrow O_2$
	CT, IL	−30.70, 0.72	−26.98, 3.36	−21.71, 1.17	−20.26, 0.79
State 9	Data link	$I_1 \rightarrow O_4$	$I_2 \rightarrow O_3$	$I_3 \rightarrow O_2$	$I_4 \rightarrow O_1$
	CT, IL	−30.70, 0.72	−27.64, 3.36	−28.44, 2.56	−29.90, 0.72

In conclusion, we propose an active non-blocking four-port optical router using four thermo-optic silicon MRRs. Device configuration and optimization of the routing elements are demonstrated. Routing topology as well as operation of the router is analyzed, and detailed characterization is performed, including spectrum, insertion loss, and crosstalk. The router has nine non-blocking routing states which can be achieved through thermo-optic effect of the silicon. According to the analysis on all the data links of the router, the insertion loss is within the range of 0.13—3.36 dB, and the crosstalk is less than −19.46 dB. The router can meet the need of large-scale ONoC.

References

[1] A. Shacham, K. Bergman and L. P. Carloni, IEEE Transactions on Computers, Analyst **57**, 1246 (2015).

[2] Y.Y. Ye, L. Duan, J. Xu, O.Y. Jin, M.K. Hung and X. Yuan, 3D Optical Networks-on-chip (NoC) for Multi-processor Systems-on-chip (MPSoC), IEEE International Conference on 3D Systems Integration, 83 (2009).

[3] Y.Y. Xie, W.H. Xu, W.L. Zhao, Y.X. Huang, T.T. Song and M. Guo, Journal of Lightwave Technology **33**, 3858 (2015).

[4] Z. Chen, H. X. Gu, Y. T. Yang, L.Y. Bai and H. Li, IEEE Computer Architecture Letters **13**, 5 (2014).

[5] Q. Q. Luo, C. T. Zheng, X. L. Huang, Y. D. Wang and D. M. Zhang, Optical and Quantum Electronics **6**, 829 (2014).

[6] C. T. Zheng, Q. Q. Luo, C. S. Ma, D. M. Zhang and Z. B. Li, Optics Communications **322**, 214 (2014).

[7] C. T. Li, C. T. Zheng, Y. Zheng, X. L. Huang, D. M. Zhang and C. S. Ma, Optics Communications **339**, 94 (2015).

[8] L. Yang, H. Jia, Y.C. Zhao and Q.S. Chen, Optics Letters **40**, 1129 (2015).

[9] R.Q. Ji, J. Xu and L. Yang, IEEE Photonics Technology Letters **25**, 492 (2013).

[10] X.F. Tan, M. Yang, L. Zhang, Y.T. Jiang and J.Y. Yang, Journal of Lightwave Technology **30**, 368 (2012).

[11] R. Min, R.Q. Ji, Q.S. Chen, L. Zhang and L. Yang, Journal of Lightwave Technology **30**, 3736 (2012).

[12] L. Zhang, Y.J. Man, X.F. Tan, M. Yang, T. Hu, J.Y. Yang and Y.T. Jiang, Journal of Optical Communications and Networking **6**, 879 (2014).

[13] C.T. Zheng, L. Liang, W.L. Ye, D.M. Zhang and C.S. Ma, IEEE Photonics Technology Letters **27**, 581 (2015).

[14] R.Q. Ji, L. Yang, L. Zhang, Y.H. Tian, J.F. Ding, H.T. Chen, Y.Y. Lu, P. Zhou and W.W. Zhu, Optics Express **19**, 18945 (2011).

[15] V.R. Shrestha, H.S. Lee, Y.G. Lee and S.S. Lee, Optics Communications **331**, 64 (2014).